Biosensors and Bioelectronics 242 (2023) 115750

Contents lists available at ScienceDirect

Biosensors and Bioelectronics

journal homepage: www.elsevier.com/locate/bios

Nano-matrixes propped self-enhanced electrochemiluminescence biosensor for microRNA detection

Weijia Sun [a], Nuo Zhang [a], Xiang Ren [a], Dan Wu [a], Yue Jia [a,**], Qin Wei [a,b,*], Huangxian Ju [a,c,***]

[a] Key Laboratory of Interfacial Reaction & Sensing Analysis in Universities of Shandong, School of Chemistry and Chemical Engineering, University of Jinan, Jinan 250022, Shandong, China
[b] Department of Chemistry, Sungkyunkwan University, Suwon 16419, Republic of Korea
[c] State Key Laboratory of Analytical Chemistry for Life Science, Department of Chemistry, Nanjing University, Nanjing 210023, China

ARTICLE INFO

Keywords:
Electrochemiluminescence
Biosensor
Self-enhancement
$Ru(dcbpy)_3^{2+}$
Nanoemitters
MicroRNA-21

ABSTRACT

MicroRNAs (miRNA) are the potential biomarker for breast cancer, a biosensor for detecting miRNA-21 was successfully prepared by covalently linking carbohydrazide (CON_4H_6) and tris (4,4 ′- dicarboxylic acid-2,2' -bipyridyl) ruthenium dichloride ($Ru(dcbpy)_3^{2+}$) as a self-enhanced emitter ($Ru–CON_4H_6$). The biosensor was prepared by coating the electrode with mesoporous silica encapsulated $Ru–CON_4H_6$ as luminophores (RMSNs) to covalently link a couple of DNA strands (Q1-H2). The RMSNs coated electrode exhibited strong ECL emission due to the intramolecular electron transfer between the electrochemically oxidized Ru $(dcbpy)_3^{2+}$ and co-reactant CON_4H_6. In the presence of target miRNA-21 and an assistant hairpin H1, H2 could be released from the surface through a strand displacement reaction (SDR), and the reserved Q1 could form G-quadruplex upon the addition of K^+. The formed G-quadruplex then interacted with Q2-Fc in the presence of Mg^{2+} to form a DNA complex on the biosensor surface, which quenched the nano-matrixes propped self-enhanced ECL emission through the electron exchange between Fc and electrode or oxidized ECL intermediates. Under optimal conditions, the ECL decrease showed a correlation with target concentration, leading to a biosensing method for sensitive detection of miRNA-21. The proposed ECL method demonstrated a detectable concentration range from 0.1 fM to 1 nM along with a detection limit of 0.03 fM, good accuracy, and acceptable reproducibility, showing that the self-enhanced ECL biosensing strategy supported by nano-matrix provided a new way for the ultrasensitive detection of miRNA, and promoted the development of breast cancer diagnosis.

1. Introduction

MicroRNAs have become one of the biomarkers of human diseases and associated with the expression of human cancer cells. Abnormal expression of microRNA-21 (miRNA-21) has been detected in solid tumors affecting different parts of the human body, including stomach, head, lung, prostate, pancreas, esophagus, colon, brain, neck, and breast (Pichler and Calin, 2015). Numerous of progressive miRNA-21 tests have been exploited utilizing sophisticated analytical techniques including northern blot, microarray, in situ hybridization (ISH) and so on (Li et al., 2020). However, the drawbacks of these methods, such as low sensitivity, complex program or poor selectivity limit their practical application in clinic diagnosis. Thus, it is an urgent need to develop fast and sensitive method for miRNA-21 detection.

Some methods have been proposed for miRNA-21 detection with the continuous exploration (Cheng et al., 2018). Among these methods, biosensors have attracted considerable attention in recent years due to their high selectivity and sensitivity for miRNA-21 analysis. As a powerful detection technique, electrochemiluminescence (ECL) has extensively been applied in disease marker detection and environmental monitoring. This technique possesses high sensitivity, low background interference (Yang et al., 2022; Richter, 2004), convenient procedure

* Corresponding author. Key Laboratory of Interfacial Reaction & Sensing Analysis in Universities of Shandong, School of Chemistry and Chemical Engineering, University of Jinan, Jinan 250022, Shandong, China.
** Corresponding author. Key Laboratory of Interfacial Reaction & Sensing Analysis in Universities of Shandong, School of Chemistry and Chemical Engineering, University of Jinan, Jinan 250022, Shandong, China.
*** Corresponding author. Key Laboratory of Interfacial Reaction & Sensing Analysis in Universities of Shandong, School of Chemistry and Chemical Engineering, University of Jinan, Jinan 250022, Shandong, China.
E-mail addresses: jykubcg@163.com (Y. Jia), sdjndxwq@163.com (Q. Wei), hxju@nju.edu.cn (H. Ju).

https://doi.org/10.1016/j.bios.2023.115750
Received 10 August 2023; Received in revised form 29 September 2023; Accepted 3 October 2023
Available online 12 October 2023

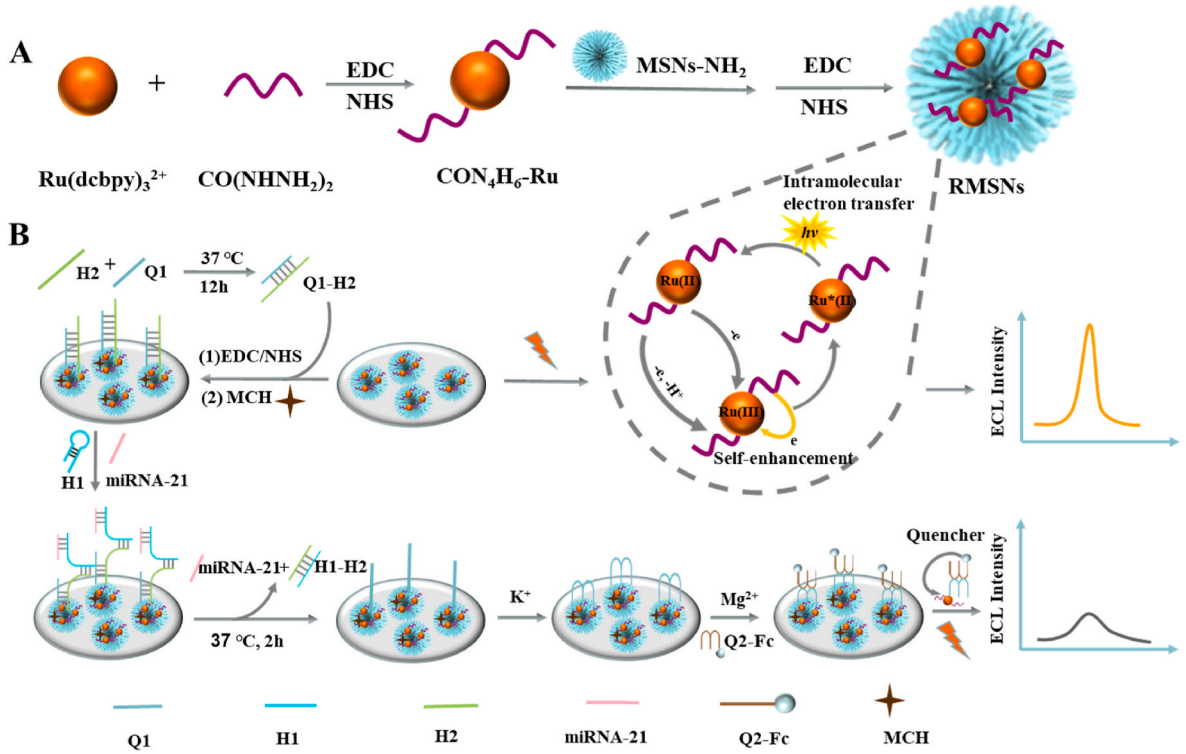

Scheme 1. (A) Synthesis process of the self-enhanced emitter and (B) the fabrication process of the biosensor.

and wide dynamic range. Different ECL emitters, such as ruthenium complexes, luminol and its derivatives, quantum dots (QDs) and metal nanoclusters (NCs), have been used ECL analysis of biomolecules (Feng et al., 2022). However, some problems such as water-solubility, slow electron transfer, low energy transfer efficiency and so on limit ECL intensity, and the stability and reproducibility of sensors (Ma et al., 2020). Some strategies, including the combination of ECL emitter with co-reactant through electrostatic interaction or covalent binding (Yang et al., 2017; Ye et al., 2019; Li et al., 2022), and the encapsulation of emitters in nanomaterials (Al-Hinaai et al., 2018; Wang et al., 2018), have been developed to improve the ECL sensing performance. These methods can not only avoid the waste of reagents and environmental pollution, but also enhance the ECL signal by shortening the electron transfer path. Among these studies, porous structures such as metal organic frameworks (MOFs) (Li et al., 2023) and covalent organic frameworks (COFs) (Luo et al., 2021) are often used as carriers of ECL emitters due to their stable frame and large specific surface area. Owing to the stable physical and chemical properties, easily surface functionality, and biocompatibility, mesoporous silica nanoparticles (MSNs) have also been used as the carriers for loading of ECL emitter (Niculescu, 2020) to improve the detection sensitivity (Kholafazad Kordasht et al., 2020). In this work, a self-enhanced emitter (Ru–CON_4H_6) was designed by covalently linking tris(4,4′-dicarboxylicacid-2,2′-bipyridyl) ruthenium (II) (Ru $(dcbpy)_3^{2+}$) with co-reactant carbohydrazide (CON_4H_6) to shorten the electron transfer pathway (Carrara et al., 2017), which was then encapsulated in MSNs to obtain RMSNs (Scheme 1A) for perfectly boosting luminous efficiency and improving the stability and reproducibility of ECL biosensors.

To achieve the biosensing application of the designed RMSNs, an ECL system was proposed for the detection of low-abundant miRNA-21 by coating RMSNs on an electrode to covalently link a couple of DNA strands (Q1-H2) and then integrate the surface strand displacement reaction (SDR), which has been used in biosynthesis (Martin-Alonso et al., 2022), drug delivery (Zhan et al., 2019), and biosensing (Jia et al., 2022) due to its dynamic characteristics and high controllability (Dai et al., 2019). The surface SDR was performed in the presence of target miRNA-21 and assistant hairpin H1, which led to the release of H2 from RMSNs coated electrode and the formation of G-quadruplex through the interaction of the retained Q1 with added K^+ (Scheme 1B). In the presence of Mg^{2+} the formed G-quadruplex could interact with Q2-Fc to form a DNA complex through π-π stacking on the biosensor surface, which quenched the nano-matrixes propped self-enhanced ECL emission through the electron exchange between Fc and electrode or oxidized ECL intermediates, leading to a target-responsive detection method. The proposed method showed excellent performance for miRNA-21 analysis, indicating promising application in clinic diagnosis.

2. Experimental section

2.1. Materials and reagents

Tris (4,4′-dicarboxylicacid-2,2′-bipyridyl) ruthenium (II) dichloride [Ru $(dcbpy)_3Cl_2$] and carbonhydrazide (CON_4H_6), tetraethyl orthosilicate (TEOS), cyclohexane, isopropanol, ethyl alcohol, (3-aminopropyl) triethoxysilane (APTES), hexadecyl trimethyl ammonium bromide (CTAB), 1-ethyl-3-(3-dimethylaminopropyl) carbodiimide hydrochloride (EDC), and N-hydroxy succinimide (NHS) were bought from Macklin Reagent Co. Ltd (Shanghai, China). Deionized (DI) water an electrical resistance of 18.25 MΩ cm^{-1} was used in the whole study. 6 × DNA loading buffer were bought from Beijing solarbio science & technology Co. Ltd. Gelred dye, DNA marker and the oligonucleotides were purchased by Sangon Biotechnology Co. Ltd (Shanghai, China). The detailed sequences were shown below.

miRNA-21: UAG CUU AUC AGA CUG AUG UUG A
H1: T CAA CAT CAG TCT GAT AAG CTA AG GGT GGG GAG GGT GGG G ATG CTA ATC
H2: CAC GAT TAG CAT CCCC ACCC TCCCC ACC CT TAG CTT ATC AGA CTG
Q1: NH_2-$(CH_2)_6$-TTT AG GGT GGG GAG GGT GGGG
Q2-Fc: Fc-TTT AG GGT GGG GAG GGT GGGG

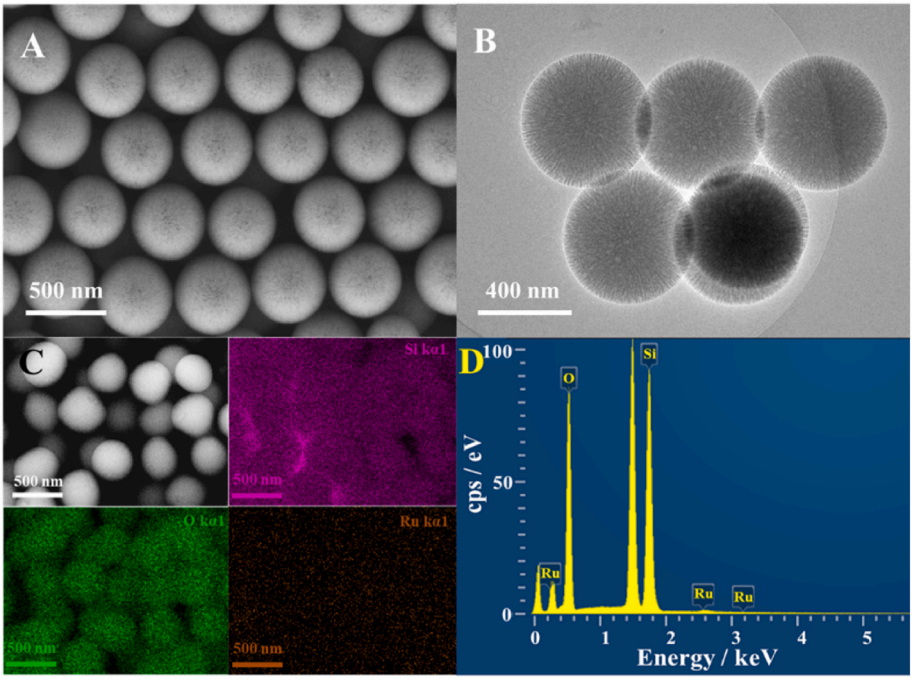

Fig. 1. (A) SEM image of MSNs. (B) TEM image of MSNs. (C) Elemental mapping images of Si, O and Ru in RMSNs. (D) EDS spectrum of RMSNs.

2.2. Preparation of Ru–CON_4H_6

62 mg of CON_4H_6 was dissolved in 4 mL of 1% acetic acid solution. 1 mL of PBS (0.1 M, pH 8.0) containing 100 mM EDC, 100 mM NHS and 4.5 mg of [Ru (dcbpy)$_3$Cl$_2$] were shaken at 4 °C for 8 h. The mixture was added with 1 mL of CON_4H_6 solution under shocking at 4 °C for 8 h to obtain Ru–CON_4H_6.

2.3. Preparation of MSNs

MSNs were synthesized by referring to a one-pot method (Sun et al., 2020). 0.5 g of CTAB and 0.2 g of carbamide were dissolved in 15 mL of water to stir for 0.5 h. 1.25 mL of TEOS, 15.0 mL of cyclohexane and 0.46 mL of isopropanol were then added in the mixture to stir at 70 °C for 16 h. After cooling to room temperature, the formed precipitate was washed with water and ethanol for three times respectively, and dried at 60 °C. Finally, the MSNs were obtained by calcining at 450 °C for 10 h.

2.4. Encapsulation of Ru in MSNs

20 mg of MSNs and 15.7 μL of APTES were dissolved in 10 mL of ethanol and added with 7.2 mL of water to stir for 0.5 h under N_2 atmosphere at room temperature. The resulting solution was centrifuged and washed for several times (Hu et al., 2018). The obtained white resultant was dried in vacuum as well as ground to obtain amino-MSNs (MSNs-NH_2). 100 μL of EDC (400 μM), 100 μL of NHS (100 μM) and 300 μL of Ru–CON_4H_6 solution were added to 1 mL of water containing 20 mg of MSNs-NH_2 to vibrate at 4 °C for 12 h. After centrifuged at 9000 rpm for 6 min, the product (RMSNs) was washed with water, dispersed in 8 mL of water and stored at 4 °C.

2.5. Fabrication of biosensor

A glassy carbon electrode (GCE, $\Phi = 4$ mm) was burnished to a glossy surface with Al_2O_3 powder, sonicated in water and dried with N_2 atmosphere. 6 μL of RMSNs dispersion was then coated on the GCE to yield a RMSNs coated electrode (RMSNs/GCE). A mixture of 10 μL of EDC (400 μM) and NHS (100 μM) mixture was then added to the surface of the modified electrode to activate the carboxyl group. Next, 10 μL of Q1-H2 (10 μM) was immobilized on the surface to obtain Q1-H2/RMSNs/GCE through covalently linking with RMSNs (Scheme 1B). After 10 μL of MCH was dropped on the surface to incubate at room temperature for 10 min to block nonspecific sites, the biosensor was obtained.

2.6. ECL detection of miRNA-21

After 10 μL of the mixture containing miRNA-21 and assistant hairpin DNA H1 (2 μM) was incubated on the biosensor surface at 37 °C for 2 h, 10 μL of K^+ solution (5 mM) was dropped on the surface at room temperature for 2 h. After that, 10 μL of Q2-Fc (2 μM) and 10 μL Mg^{2+} (5 mM) were dropped on the biosensor to incubate at 37 °C for 2 h. The resulting biosensor was used for ECL measurement in 10 mL of 0.1 M PBS (pH 8.0).

3. Results and discussion

3.1. Characterization of MSNs

The structure of MSNs was characterized with X-ray diffraction (XRD) pattern, which showed a diffraction peak at the 2θ of 23° (Fig. S1), confirming an amorphous structure (Yin et al., 2021). The scanning electron microscopic (SEM) image of MSNs showed a spherical morphology with uniform dimension of about 500 nm and arranged like matrixes (Fig. 1A). In order to better observe the interior of the particles, the transmission electron microscopic (TEM) image was taken, which showed a porous structure (Fig. 1B), providing a possibility for packaging of luminophores. After encapsulating Ru–CON_4H_6 in MSNs, the element mapping images showed the uniform distribution of Si, O and Ru elements in the spherical area (Fig. 1C), and these elements were also observed from energy dispersive spectrum (EDS) (Fig. 1D).

To explore the amount of Ru encapsulated in RMSNs, the Ru concentration of 30 mL of RMSNs dispersion was quantified using inductively coupled plasma optical emission spectrometer (ICP-OES) and the correction curve (Fig. S2). The results were listed in Table S1. The encapsulation efficiency (%) of Ru was about 42.6%. The FT-IR spectrum of MSNs showed an intense peak at 1017 cm^{-1} and a slightly lower

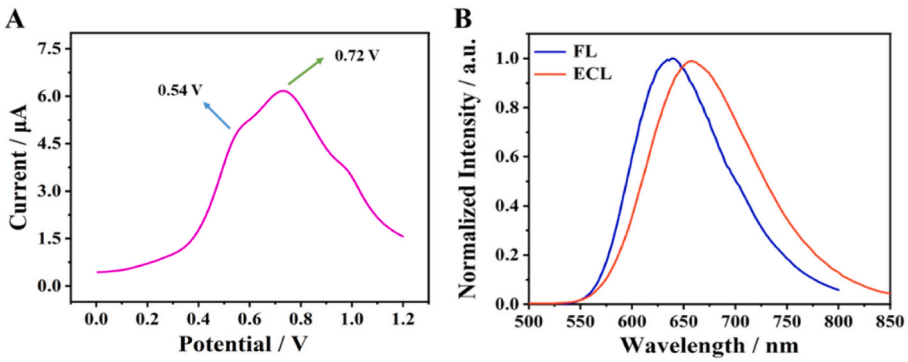

Fig. 2. (A) DPV profile of RMSNs-modified GCE in 10 mL of PBS (0.1 M, pH 8.0) from 0 to +1.2 V. (B) Normalized FL spectrum of RMSNs and normalized ECL spectrum of RMSNs-modified GCE in 10 mL of PBS (0.1 M, pH 8.0).

peak at 460 cm^{-1} (Fig. S3), which were attributed to the Si–O–Si asymmetric (vas) stretching vibration of SiO_2 matrix. After amination, the MSNs-NH_2 showed an absorption peak of N–H deformation vibration at 1637 cm^{-1} (Hu et al., 2016). A characteristic absorption band with peak at 3200 cm^{-1} might be concealed to the strong absorption of O–H and Si–O vibration. These results demonstrated the successful synthesis of MSNs and MSNs-NH_2. The porous nature of MSNs before and after loading emitters was confirmed by the type-IV isotherm of N2 adsorption-desorption isotherm (Fig. S4). According to the Brouwer -Emmet-Teller (BET) test results, the surface area of MSNs before loading emitters was 934.46 m^2/g, the pore volume was 0.644 cm^3/g, and the average pore size of BJH was 4.72 nm. The surface area of the loading emitters was 123.2 m^2/g, the pore volume was 0.197 cm^3/g, and the average pore size of the BJH was 3.12 nm. According to the above results, it was shown that MSNs had porous structure. To demonstrate the electrochemical surface area, RMSNs modified GCE was tested using $[Fe(CN)_6]^{4-/3-}$ as redox indicator at different scanning rates (Fig. S5). The effective electrochemical surface area could be calculated to be about 0.12 cm^2. The specific calculation process was further presented in the Supplementary Material.

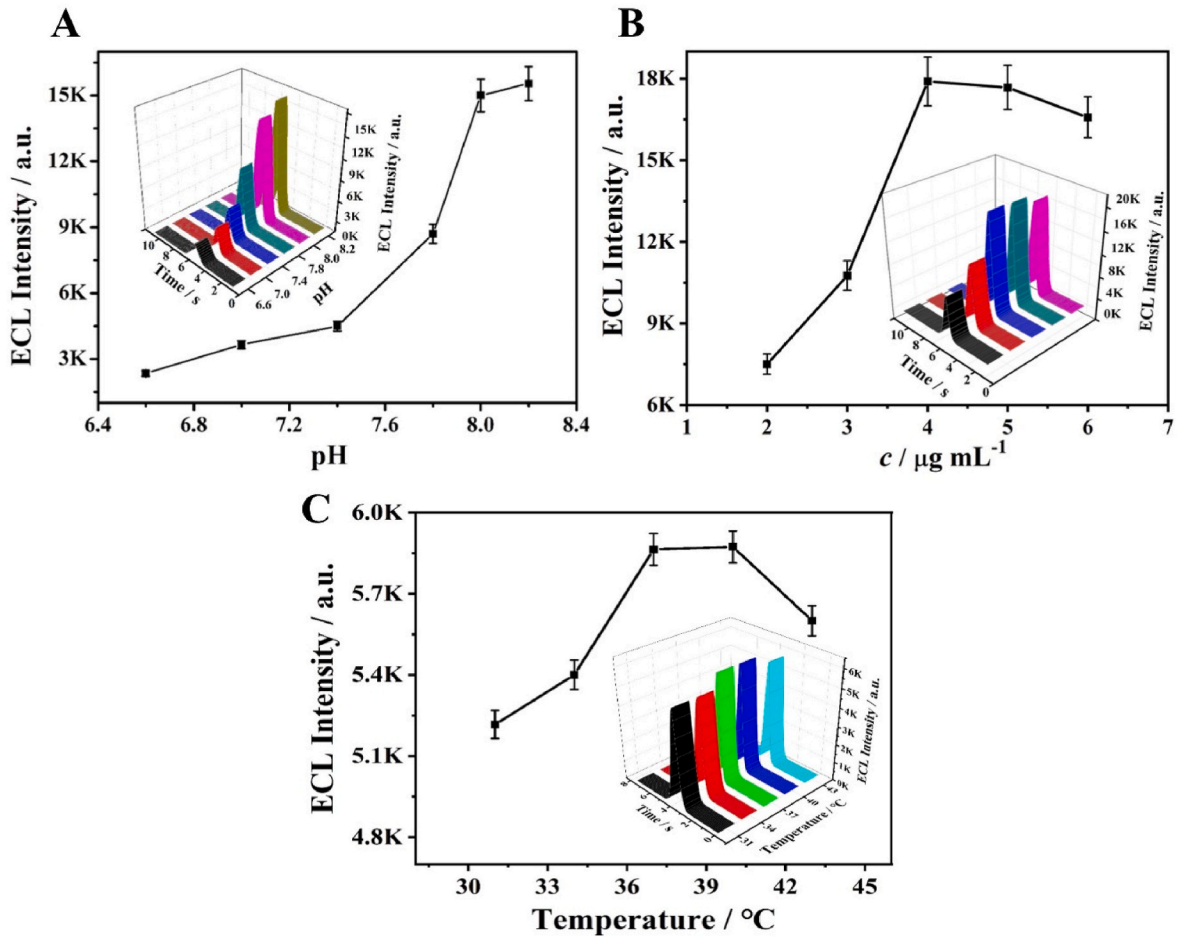

Fig. 3. (A) Optimization of pH of PBS, (B) Ru concentration in 8 mL RMSNs solution containing 20 mg MSNs and (C) the ECL performance for 1 pM miRNA detection at different incubation temperatures. (Error bars: ±standard deviation (SD), $n = 5$).

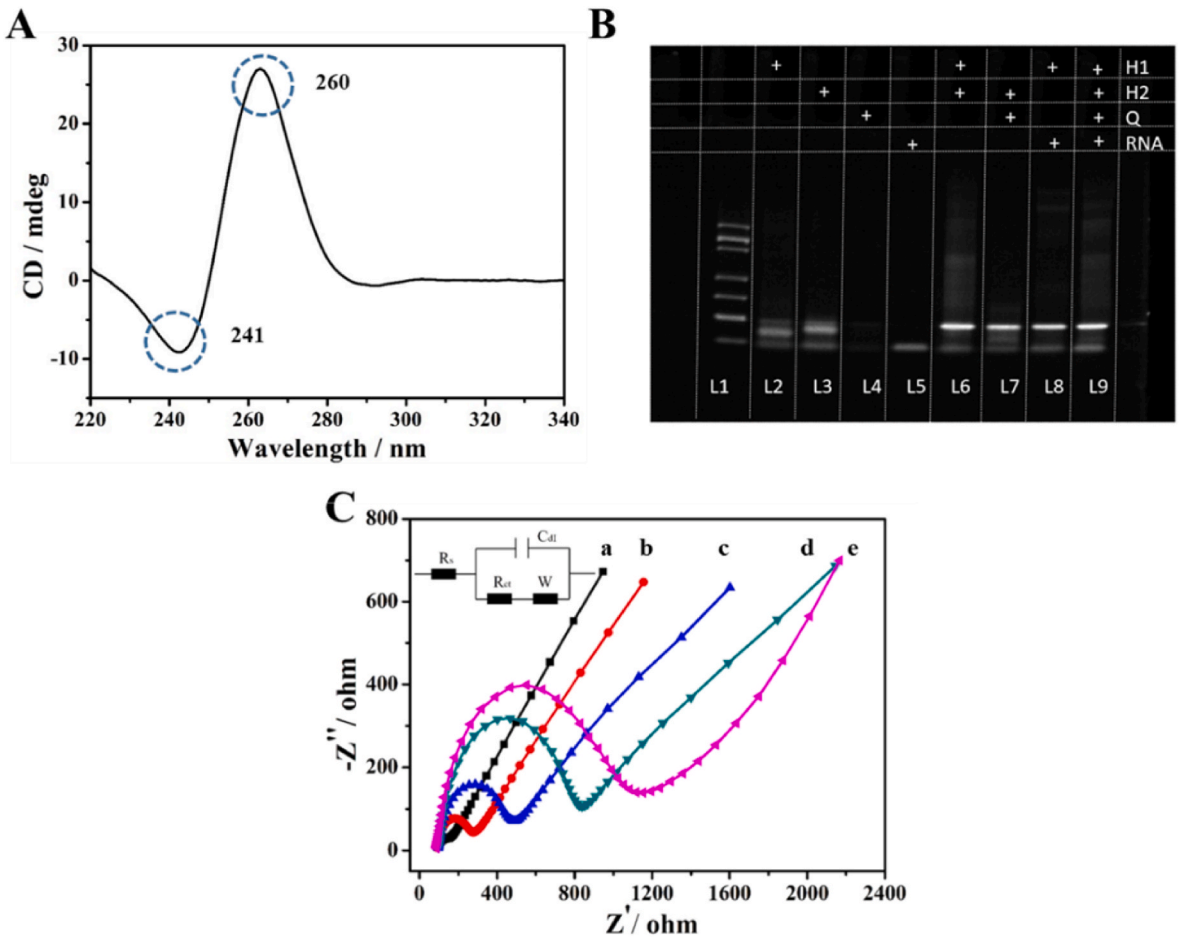

Fig. 4. (A) CD spectrum of G-quadruplexes structure formed at 0.5 mM K^+. (B) PAGE image of marker (L1), 10 μM H1 (L2), 10 μM H2 (L3), 10 μM Q1 (L4), 10 μM miRNA-21 (L5), 10 μM H1 + 10 μM H2 (L6), 10 μM H2 + 10 μM Q1 (L7), 10 μM miRNA-21 + 10 μM H1 (L8), 5 μM H1 + 5 μM H2 + 5 μM Q1 + 5 μM miRNA-21 (L9). (C) EIS profiles of bare GCE (a), RMSNs/GCE (b), Q1-H2/RMSNs/GCE (c), MCH/Q1-H2/RMSNs/GCE (d), and H1-miRNA-21/MCH/Q1-H2/RMSNs/GCE (e) in 5.0 mmol/L $[Fe(CN)_6]^{-3/-4}$ and 0.1 mol/L KCL.

3.2. Possible ECL mechanism

In order to explore the oxidation process of Ru–CON_4H_6, the differential pulse voltammetric (DPV) curve and ECL spectrum of RMSNs-modified GCE in 10 mL of PBS were recoded. The DPV profile showed two oxidation processes near +0.54 V and +0.72 V respectively (Fig. 2A), which were related to the oxidation of CON_4H_6 and Ru $(dcbpy)_3^{2+}$, respectively (Fu et al., 2020). The ECL emission peak of RMSNs occurred at 658 nm, which was 18 nm redder than the fluorescence (FL) emission peak of 640 nm for RMSNs (Fig. 2B). The red shift indicated that the surface of RMSNs was not completely passivated and existed surface defects, which led to surface-state ECL emission of RMSNs (Feng et al., 2022).

Compared with the ECL emission of MSNs@Ru-modified GCE in PBS containing 5 mg/mL CON_4H_6, here MSNs@Ru were Ru $(dcbpy)_3^{2+}$ encapsulated MSNs, the ECL emission of RMSNs-modified GCE under the same detection conditions and Ru $(dcbpy)_3^{2+}$ amount showed approximately 60 times higher (Fig. S6). Furthermore, the oxidation of RMSNs occurred at lower potential than that of MSNs@Ru. The luminescence mechanism was further verified by density functional theory (DFT). The singlet and triplet excitation energies at PBE0/def2SVP levels were calculated by TDDFT method to obtain highest occupied molecular orbital (HOMO) and lower unoccupied molecular orbital (LUMO) energy levels (Adamo and Barone, 1999; Le Duff and Ouillon, 1985). As shown in Fig. S7, The LUMO level of CON_4H_6 was higher than that of Ru $(dcbpy)_3^{2+}$, which proved that CON_4H_6 may transfer electrons to Ru $(dcbpy)_3^{2+}$. CON_4H_6 was first excited to its S1 with an excitation energy of 6.82 eV, after which the energy transferred (ET) to the singlet state (S1) of Ru $(dcbpy)_3^{2+}$ and to T1 via the intersystem crossover (ISC), and then to the ground state (S0) by a radiative transition from T1 to produce luminescence (Zhu et al., 2021; Zhao et al., 2022). The self-enhanced ECL emission could be attributed to the intramolecular electron transfer as shown in Scheme 1 along with following equations (Richter, 2004; Xue et al., 2020):

$$CON_4H_6\text{–Ru (II)} - 2e^- \rightarrow CON_4H_6^{\bullet+} - \text{Ru (III)} \quad (1)$$

$$CON_4H_6^{\bullet+}\text{-Ru (III)} - H^+ \rightarrow CON_4H_6^{\bullet}\text{-Ru (III)} \quad (2)$$

$$CON_4H_6^{\bullet}\text{-Ru (III)} \rightarrow CON_4H_6\text{– Ru*(II)} \quad (3)$$

$$CON_4H_6\text{– Ru*(II)} \rightarrow CON_4H_6\text{–Ru (II)} + h\nu \quad (4)$$

3.3. Optimization of ECL conditions

The exploration of optimal conditions is of great importance for a new ECL system. The oxidation of CON_4H_6 as a type of amine co-reactant involved the participation of proton, thus pH of detection solution could influence the ECL response. With the increasing pH, the ECL intensity increased and reached the maximum value at pH 8.0 (Fig. 3A), indicating weak alkaline environment could facilitate the deprotonation process of oxidized amine co-reactant (Yin et al., 2008). Thus pH 8.0 was

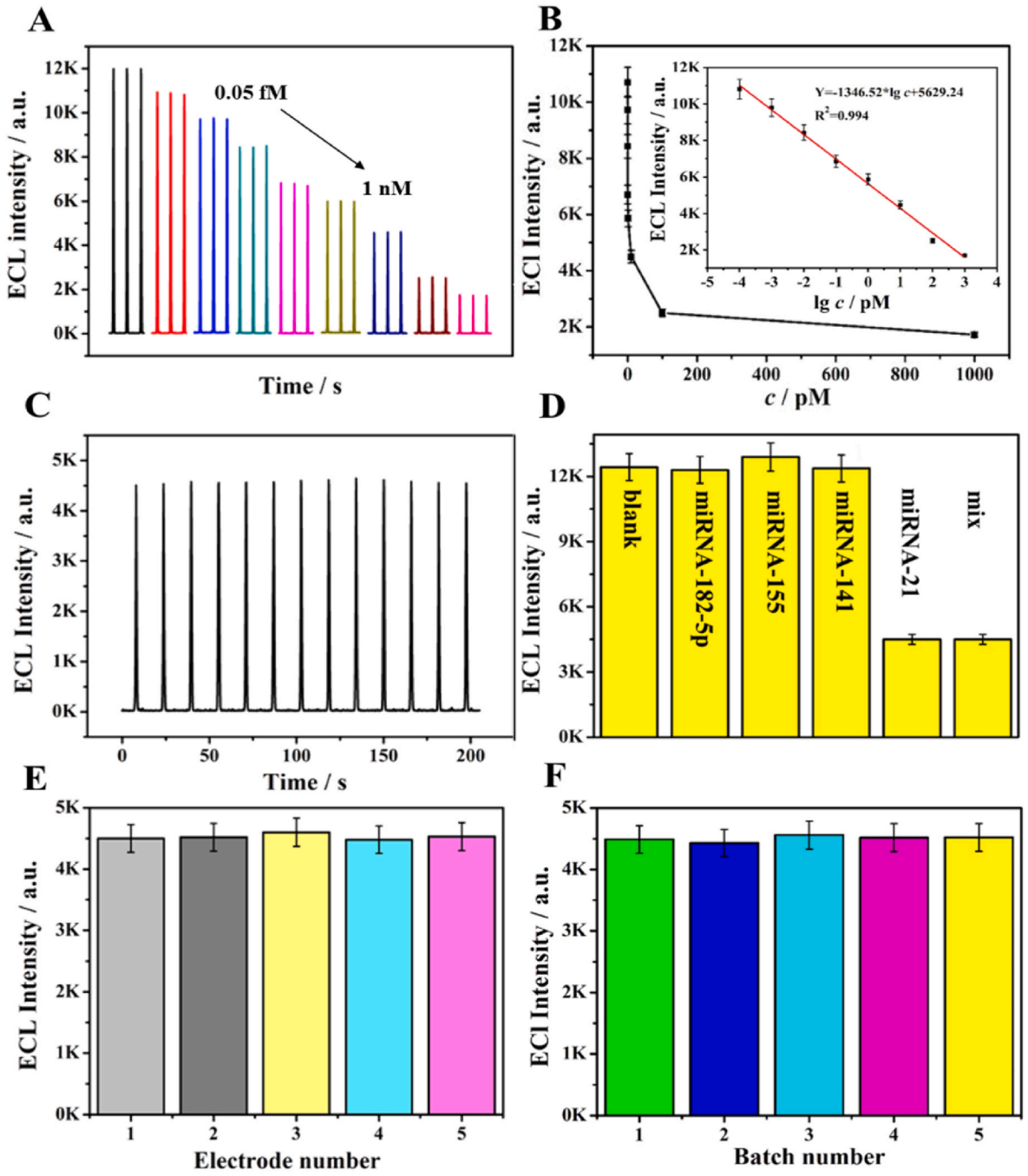

Fig. 5. (A) ECL-time curves of ECL biosensor at different concentrations of miRNA-21 (from 0.05 fM to 1.0 nM). (B) Calibration curve for miRNA-21 detection. (C) Biosensing stability for 10 pM miRNA-21. (D) Specificity of the biosensing method tested with blank (PBS), 1.0 nM miRNA-182–5p, 1.0 nM miRNA-155, 1.0 nM miRNA-141, 10 pM miRNA-21 and mixture of 10 pM miRNA-21, 1.0 nM miRNA-182–5p, 1.0 nM miRNA-155 and 1.0 nM miRNA-141. (E, F) Preparation reproducibility of ECL biosensors with the same (E) and different batches (F) at 10 pM miRNA-21. (Error bars: ±SD), $n = 5$).

chosen as the optimal detection condition. The amount of Ru in RMSNs depended on its concentration used for RMSNs preparation. At the concentration of 4 μg/mL the ECL intensity of RMSNs showed the maximum value (Fig. 3B). Thus, the optimal concentration of Ru was 4 μg/mL. To explore the influence of temperature on sensing performance, five incubation temperatures were selected for exploration. As shown in Figs. 3C and 37 °C was the optimal incubation temperature for the sensor. At this temperature, it would maintain the activity of the biomolecule to the greatest extent possible, enabling precise detection of miRNA-21.

3.4. Circular dichroism and polyacrylamide gel electrophoresis analysis

Circular dichroism (CD) analysis was utilized to verify the formation of the G-quadruplex under the action of K^+. The CD spectrum of the G-quadruplex formed at 0.5 mM K^+ showed a positive absorption peak at 260 nm (Fig. 4A). It was consistent with the conformation of continuous guanine ribonucleotide which formed the core structure of G-quadruplex. The emergence of the negative peak at 241 nm was generally attributed to the formation of the G-quadruplex conformation, which was in good agreement with prior investigative results (Martadinata and Phan, 2009).

Polyacrylamide gel electrophoresis (PAGE) experiments were

Table 1
Performance comparation of this proposed method with previously reported methods for miRNA detection.

Analytical method	Linear range	LOD	Ref.
ICP-MS	0.02 nM–1 nM	5 pM	(Kang et al., 2021)
SERs	0.33 fM-3.3 pM	42 aM	(Yao et al., 2021)
EIS	1 pM-1 nM	0.3 pM	(Azzouzi et al., 2017)
FL	1 fM-1 pM	1 fM	(He et al., 2022)
Electrochemical	1 fM-100 pM	0.16 fM	(Ouyang et al., 2023)
FRET	3 pM–500 pM	80 fM	(Xu et al., 2021)
Electrochemical	2 fM-0.1 nM	1.24 fM	(Khodadoust et al., 2023)
ECL	0.1 fM-1 nM	0.03 fM	This work

conducted to certify the feasibility of SDR and the formation of double-stranded DNA. In Fig. 4B, L2-L5 correspond to the bands of H1, H2, Q1 and miRNA-21 respectively. After H1 was mixed with H2 to react for 2 h at 37 °C, a new band occurred at slower migration rate (L6), which was attributed the formation of H1–H2 via complementary base pairing. Due to the existence of complementary base pairs between Q1 and H2, as well as between H1 and miRNA-21, Q1-H2 and H1-miRNA-21 could be formed (L7 and L8) after mixing respectively according to the principle of complementary base pairing. miRNA-21 was replaced by H1 to form a more stable double stranded DNA H1–H2 after mixing solutions containing Q1-H2 and H1 miRNA-21 due to the presence of more complementary base pairs in H1 and H2. Q1 existed in the form of a single strand. Due to the slight difference in the number of bases between Q1 and miRNA-21, resulting in only two bands being displayed (L9), corresponding to the bands of Q1 (L4), miRNA-21 (L5), and H1–H2 (L6) when they existed alone, which proved the occurrence of the SDR and the feasibility of the biosensing strategy.

3.5. Characterization of biosensor construction and miRNA-21 recognition

The successful construction of the biosensor and the detection procedure were confirmed by electrochemical impedance spectroscopy (EIS). The electron-transfer resistance (R_{et}) was reflected in the Nyquist plots through the semicircle diameter in the high frequency region. As shown in Fig. 4C, the R_{et} increased to 300 Ω on account of weak electrical conductivity when the RMSNs were coated on the electrode surface (curve b). After the modification of Q1-H2, the steric hindrance increased and the R_{et} of the modified electrode increased obviously (curve c). The R_{et} showed continuous augmentation after being modified with MCH and then recognition with miRNA-21-H1 (curves d and e), which preliminarily proved the successful preparation of biosensor for the detection of miRNA-21.

3.6. ECL performance of the biosensor

Under optimal conditions, the constructed biosensor was used to detect miRNA-21. Upon its recognition to miRNA-21 in the presence of assistant hairpin H1, and following incubation with K^+ solution, and the mixture of Q2-Fc and Mg^{2+} respectively, the ECL emission intensity decreased. Moreover, the decrease value increased with the increasing concentration of miRNA-21 (Fig. 5A), which showed a linear plot of ECL intensity decrease vs the logarithm of miRNA-21 concentration ranging from 0.1 fM to 1.0 nM ($R^2 = 0.994$) (Fig. 5B). The ECL decrease could be attributed to the oxidation of Fc formed the Fc^+, which reacted with [Ru $(dcbpy)_3^{2+}$]* to block the generation of ECL signal. A series of metal complexes could quench the luminescence of Ru $(dcbpy)_3^{2+}$ through resonance energy transfer (RET) or electron transfer. By comparing the ECL spectral emission of Ru–CON_4H_6 with the UV–vis absorption spectrum of Fc solution in Fig. S8, it was found that there was no matching part, which rules out the suspicion of quenching luminescence by RET. It was also considered as a charge transfer quenching mechanism in previous studies. (Cao et al., 2006; Deng et al., 2013).

$$Fc - e \rightarrow Fc^+ \quad (5)$$

$$Fc^+ + CON_4H_6\text{–}\ Ru^*(II) \rightarrow Fc + CON_4H_6\text{–}Ru\ (III) \quad (6)$$

From the linear plot and 3 times relative standard deviation measured at blank, the limit of detection (LOD) of this system was obtained to be about 0.03 fM. Compared with the previously reported methods, the proposed method showed lower LOD (Table 1). The operational stability of the proposed biosensor was examined at 10 pM miRNA-21. The ECL intensities with continuous 13 measurements gave a relative standard deviation (RSD) of 0.80% (Fig. 5C), indicating good operational stability. The specificity of the constructed system for the detection of miRNA-21 was evaluated with its ECL responses to different miRNAs (miRNA-182–5p, miRNA-155, miRNA-141) at 1 nM. In the absence of miRNA-21, the ECL intensity of the biosensor after treated with these miRNAs according to the detection procedure showed little difference from that of blank. Only miRNA-21 (10 pM) and its mixture with other miRNAs resulted in the same decrease of ECL intensity (Fig. 5D), indicating good selectivity. The repeatability of this biosensor was tested with intra and inter precision for 10 pM miRNA-21 detection. The former was tested with five different biosensors prepared in the same batch (Fig. 5E), and the latter was tested with five different batches of biosensors (Fig. 5F), which showed the RSDs of 1.0% and 1.1%, respectively, indicating exceptional reproducibility.

3.7. Analysis of real samples

In order to estimate the feasibility of this proposed biosensor in real sample analysis, the standard addition recovery measurements were performed by spiking miRNA-21 in human serum samples. The recovery was in the range of 96.0–102%, and the RSD ranged from 3.2% to 4.3% (Table S2), indicating that the proposed biosensing method could be used for detecting miRNA-21 in biological samples.

4. Conclusions

A self-enhanced ECL emitter has been designed by covalently linking Ru $(dcbpy)_3^{2+}$ with coreactant CON_4H_6, and encapsulated in MSNs for ECL biosensing, which leads to 60 times stronger ECL intensity than Ru $(dcbpy)_3^{2+}$ encapsulated MSNs at the same conditions. An ECL biosensing method for miRNA-21 has also been proposed with the nanomatrixes propped self-enhanced ECL emitter by integrating the surface strand displacement reaction, the formation of G-quadruplex and its interaction with Q2-Fc as quencher. The surface-state ECL emission mechanism of RMSNs and the biosensing mechanism have been demonstrated. The proposed ECL method possesses wide detectable concentration range along with a detection limit down to 0.03 fM, good stability, acceptable reproducibility and specificity, showing promising application in bioanalysis.

CRediT authorship contribution statement

Weijia Sun: Conceptualization, Data curation, Writing – original draft. **Nuo Zhang:** Methodology, Data curation, Funding acquisition. **Xiang Ren:** Methodology, Writing – review & editing. **Dan Wu:** Methodology, Writing – review & editing. **Yue Jia:** Writing – review & editing. **Qin Wei:** Supervision, Funding acquisition, Project administration. **Huangxian Ju:** Writing – review & editing, Formal analysis, Project administration.

Declaration of competing interest

The authors declare that they have no known competing financial interests or personal relationships that could have appeared to influence the work reported in this paper.

Data availability

Data will be made available on request.

Acknowledgements

This study was supported by the National Natural Science Foundation of China (Nos.22274062, 22206056), the Natural Science Foundation of Shandong Province (ZR2020QB097, ZR2022QB117). The authors thank Tianwei Lin from Shiyanjia Lab (www.shiyanjia.com) for the DFT analysis.

Appendix A. Supplementary data

Supplementary data to this article can be found online at https://doi.org/10.1016/j.bios.2023.115750.

References

Adamo, C., Barone, V., 1999. J. Chem. Phys. 110 (13), 6158–6170.
Al-Hinaai, M.M., Kyaw, H.H., Al-Harthi, S.H., Khudaish, E.A., 2018. Sens. Actuators B-Chem. 257, 460–468.
Azzouzi, S., Mak, W.C., Kor, K., Turner, A.P.F., Ali, M.B., Beni, V., 2017. Biosens. Bioelectron. 92, 154–161.
Cao, W., Ferrance, J.P., Demas, J., Landers, J.P., 2006. J. Am. Chem. Soc. 128 (23), 7572–7578.
Carrara, S., Arcudi, F., Prato, M., De Cola, L., 2017. Angew. Chem. Int. Ed. 56 (17), 4891, 4891.
Cheng, Y., Dong, L., Zhang, J., Zhao, Y., Li, Z., 2018. Analyst 143 (8), 1758–1774.
Dai, Y., Furst, A., Liu, C.C., 2019. Trends Biotechnol. 37 (12), 1367–1382.
Deng, S., Lei, J., Liu, Y., Huang, Y., Ju, H., 2013. Chem. Commun. 49 (21), 2106–2108.
Feng, Y., Wang, N., Ju, H., 2022. Sci. China Chem. 65 (12), 2417–2436.
Fu, L., Zhang, B., Fu, K., Gao, X., Zou, G., 2020. Anal. Chem. 92 (8), 6144–6149.
He, M., Shang, N., Zheng, B., Yue, G., Han, X., Hu, X., 2022. Mikrochim. Acta 189 (6), 217.
Hu, H., Arena, F., Gianolio, E., Boffa, C., Di Gregorio, E., Stefania, R., Orio, L., Baroni, S., Aime, S., 2016. Nanoscale 8 (13), 7094–7104.
Hu, S., Shao, S., Chen, H., Sun, J., Zhai, J., Zheng, H., Wan, M., Liu, Y., Mao, C., Zhao, J., 2018. J. Phys. Chem. C 122 (17), 9680–9687.
Jia, Y., Zhang, N., Du, Y., Ren, X., Ma, H., Wu, D., Fan, D., Wei, Q., Ju, H., 2022. Biosens. Bioelectron. 210, 114291.
Kang, Q., He, M., Chen, B., Hu, B., 2021. Sens. Actuators B-Chem 345.
Khodadoust, A., Nasirizadeh, N., Seyfati, S.M., Taheri, R.A., Ghanei, M., Bagheri, H., 2023. Talanta 252, 123863.
Kholafazad Kordasht, H., Pazhuhi, M., Pashazadeh-Panahi, P., Hasanzadeh, M., Shadjou, N., 2020. Trends Anal. Chem. 124.
Le Duff, Y., Ouillon, R., 1985. J. Chem. Phys. 82 (1), 1–4.
Li, Q., Zhou, S., Zhang, T., Zheng, B., Tang, H., 2020. Biosens. Bioelectron. 150, 111866.
Li, L., Zhao, W., Zhang, J., Luo, L., Liu, X., Li, X., You, T., Zhao, C., 2022. J. Colloid Interface Sci. 608, 1151–1161.
Li, X., Ren, X., Yang, L., Wang, W., Fan, D., Kuang, X., Sun, X., Wei, Q., Ju, H., 2023. Sens. Actuators B-Chem. 378.
Luo, R., Lv, H., Liao, Q., Wang, N., Yang, J., Li, Y., Xi, K., Wu, X., Ju, H., Lei, J., 2021. Nat. Commun. 12 (1), 6808.
Ma, C., Cao, Y., Gou, X., Zhu, J.J., 2020. Anal. Chem. 92 (1), 431–454.
Martadinata, H., Phan, A.T., 2009. J. Am. Chem. Soc. 131 (7), 2570–2578.
Martin-Alonso, S., Kang, D., Martinez Del Rio, J., Luczkowiak, J., Frutos-Beltran, E., Zhang, L., Cheng, X., Liu, X., Zhan, P., Menendez-Arias, L., 2022. J. Mol. Biol. 434 (7), 167507.
Niculescu, V.-C., 2020. Front. Mater. 7.
Ouyang, R., Jiang, L., Xie, X., Yuan, P., Zhao, Y., Li, Y., Tamayo, A.I.B., Liu, B., Miao, Y., 2023. Mikrochim. Acta 190 (2), 52.
Pichler, M., Calin, G.A., 2015. Br. J. Cancer 113 (4), 569–573.
Richter, M.M., 2004. Chem. Rev. 104 (6), 3003–3036.
Sun, Y., Zhu, X., Liu, H., Dai, Y., Han, R., Gao, D., Luo, C., Wang, X., Wei, Q., 2020. ACS Appl. Mater. Interfaces 12 (5), 5569–5577.
Wang, F., Lin, J., Yu, S., Cui, X., Ali, A., Wu, T., Liu, Y., 2018. ACS Appl. Mater. Interfaces 10 (44), 38223–38229.
Xu, J., Qiu, X., Hildebrandt, N., 2021. Nano Lett. 21 (11), 4802–4808.
Xue, J., Jia, Y., Yang, L., Feng, J., Wu, D., Ren, X., Du, Y., Ju, H., Wei, Q., 2020. Anal. Chem. 92 (20), 14203–14209.
Yang, H.-Y., Wang, H.-J., Xiong, C.-Y., Chai, Y.-Q., Yuan, R., 2017. ACS Appl. Mater. Interfaces 9 (41), 36239–36246.
Yang, E., Zhang, Y., Shen, Y., 2022. Anal. Chim. Acta 1209, 339140.
Yao, Y., Zhang, H., Tian, T., Liu, Y., Zhu, R., Ji, J., Liu, B., 2021. Talanta 235, 122728.
Ye, J., Liu, G., Yan, M., Zhu, Q., Zhu, L., Huang, J., Yang, X., 2019. Anal. Chem. 91 (20), 13237–13243.
Yin, X.-B., Sha, B.-B., Zhang, X.-H., He, X.-W., Xie, H., 2008. Electroanalysis 20 (10), 1085–1091.
Yin, Z., Ji, Q., Wu, D., Li, Z., Fan, M., Zhang, H., Zhao, X., Wu, A., Cheng, L., Zeng, L., 2021. ACS Appl. Mater. Interfaces 13 (13), 14928–14937.
Zhan, Q., Shi, X., Zhou, J., Zhou, L., Wei, S., 2019. Small 15 (3), e1803926.
Zhao, L., Song, X., Wang, H., Wang, X., Wu, D., Wei, Q., Ju, H., 2022. Chem. Eng. J. 446.
Zhu, D., Zhang, Y., Bao, S., Wang, N., Yu, S., Luo, R., Ma, J., Ju, H., Lei, J., 2021. J. Am. Chem. Soc. 143 (8), 3049–3053.